Theoretical Study of Sc^{2+}, Ti^{2+}, V^{2+}, Cr^{2+}, and Mn^{2+} Bound to H_2†

James F. Harrison* and Joseph P. Kenny‡

Department of Chemistry, Michigan State University, East Lansing, Michigan 48824-1322

Received: February 19, 2002; In Final Form: September 3, 2002

The binding energies, vibration frequencies, and geometry of the high spin complexes of the dipositive transition metals, Sc^{2+}, Ti^{2+}, V^{2+}, Cr^{2+}, and Mn^{2+}, with molecular H_2 have been determined for all states correlating to the lowest term of the dipositive ion using multireference CI techniques. As expected, the bonding in these complexes is dominated by electrostatics (that is, enhanced by electron correlation) and varies smoothly across the sequence from Sc to Mn. The high spin complexes for Sc^{2+}, Ti^{2+}, V^{2+}, and Mn^{2+} are the thermodynamic ground states for the MH_2^{2+} system. For Cr^{2+}, however, the large second ionization energy of Cr results in the charge exchange reaction $Cr^{2+} + H_2 \rightarrow Cr^+ + H_2^+$ being competitive with the electrostatic complex. The computed properties are compared with those for the corresponding monopositive ions.

Introduction

Although there have been many theoretical and experimental studies[1−18] of the interaction between a monopositive first row transition metal ion (M^+) and molecular hydrogen, no studies on the interaction of dipositive transition metal ions (M^{2+}) with H_2 have been reported. Given what has been learned from the reaction of M^+ with H_2, one expects that the lowest exothermic product of an early transition metal dipositive ion, M^{2+}, with H_2 will be a complex with the spin corresponding to the lowest term of the $3d^n$ configuration of M^{2+} and essentially intact H_2. We collect the energy of the various products relative to M^{2+} and H_2 in Table 1, and interestingly, the high spin complex seems to be the lowest energy product for all metals. The binding energies of MH^{2+} and MH^+ that go into the construction of this table are from the review by Harrison.[19] The only reaction that comes close to competing for the ground-state process is the charge exchange reaction

$$Cr^{2+} + H_2 \rightarrow Cr^+ + H_2^+, \quad \Delta E = -1.06 \text{ eV}$$

that is comparable in exothermicity to (vide infra)

$$Cr^{2+} + H_2 \rightarrow CrH_2^{2+}, \quad \Delta E = -1.10 \text{ eV}$$

In preliminary studies, we could not find any low spin, covalently bound states of MH_2^{2+} that were lower, or even comparable, in energy to the high spin state.

This study is concerned with determining the binding energy, geometry, and vibration frequencies of the low lying molecular states of MH_2^{2+} correlating with the magnetic sublevels of the lowest term of M^{2+}. Additionally, we will compare the properties of the dipositive molecular ions with those of their monopositive counterparts. We restrict this initial study to the early first row transition elements and will discuss the latter elements and the complexities that doubly occupied d orbitals present in a future publication.

Calculations

The transition metal basis set is the large atomic natural orbital (ANO) set developed by Bauschlicher[20] and Partridge[21] and is contracted to [7s6p4d3f2g], whereas the H basis is the AVQZ set of Dunning et al.[22] with the f orbitals removed, contracted to [4s3p2d]. The calculations were done using the program MOLPRO[23] developed by Werner and Knowles. The orbitals used in the internally contracted mulireference CI were obtained from a CASSCF calculation on the electronic state of interest in C_{2v} symmetry. When two states of the same symmetry are studied, we generate the orbitals via a state averaged CASSCF. The basis set is sufficiently large that basis set superposition errors are not expected to be important and counterpoise corrections for selected states confirm this. Spectroscopic constants and wave function amplitudes were obtained with locally written codes.

Discussion

The similarity of the parallel and perpendicular components of the polarizability[24] of H_2 and its positive quadrupole moment[25] ensures that H_2 will bind side on[4] to M^{2+} resulting in a C_{2v} complex. Accordingly, we place M^{2+} at the origin of our coordinate system with H_2 in the *yz* plane with *z* as the C_2 axis. The 3d orbitals on M^{2+} have the symmetries, d_{z^2} (a_1), d_{xz} (b_1), d_{yz} (b_2), d_{xy} (a_2), and $d_{x^2-y^2}$ (a_1) and in what follows are referred to as d_σ, $d\pi_x$, $d\pi_y$, d_-, and d_+. As H_2 approaches M^{2+} in this symmetry, the degeneracy of the lowest term splits as shown in Table 2. Note that the magnetic sublevels of the Sc^{2+}, Cr^{2+}, and Mn^{2+} terms may be represented by a single determinant at the Hartree−Fock level, whereas a multi determinant representation is needed for Ti^{2+} and V^{2+}. The orbital composition for these two terms is shown in Tables 3 and 4.

The actual splitting of the terms is shown in Figure 1, whereas the binding energies, geometries, and vibration frequencies are collected in Tables 5−8. In all cases, the σ_g bonding orbital of H_2 interacts with the metal $3d_\sigma$ orbital resulting in a bonding and antibonding orbital pair. The bonding orbital is primarily the H_2 σ_g orbital in which some $3d_\sigma$ orbital mixes constructively, whereas the antibonding orbital is primarily metal $3d_\sigma$ with an

† Part of the special issue "Jack Beauchamp Festschrift".

* To whom correspondence should be addressed.

‡ Current address: Center for Computational Quantum Chemistry, 1001 Cedar Street, University of Georgia, Athens, GA 30602-2556.

10.1021/jp0204612 CCC: $22.00
Published on Web 09/25/2002

TABLE 1: Energy (eV) of Possible High-Spin Products of $M^{2+} + H_2$[a]

	$M^{2+} + 2H^{\bullet}$	$M^{+} + H^{+} + H^{\bullet}$	$MH^{+} + H^{\bullet}$	$MH^{2+} + H^{\bullet}$	$M^{+} + H_2^{+}$	$M - H_2^{2+}$
Sc	4.48	5.19	2.79	3.13	2.54	−0.58
Ti	4.48	4.45	2.14	3.62	1.80	−0.68
V	4.48	3.88	1.83	3.77	1.44	−0.91
Cr	4.48	1.59	0.22	3.55	−1.06	−1.10
Mn	4.48	2.44	0.38	3.74	−0.21	−0.88

[a] Negative entries correspond to exothermic products.

TABLE 2: Symmetry Reduction as H_2 Approaches M^{2+} in C_{2v} Symmetry

ion	term	$C_{\infty v}$	C_{2v}
Sc^{2+} (d)	^2D	$^2\Delta$	$^2A_1(\delta_+),^2A_2(\delta_-)$
		$^2\Pi$	$^2B_1(\pi_x),^2B_2(\pi_y)$
		$^2\Sigma^+$	$^2A_1(\sigma)$
Ti^{2+} (d^2)	^3F	$^3\Phi$	$^3B_1,^3B_2$
		$^3\Delta$	$^3A_1,^3A_2$
		$^3\Pi$	$^3B_1,^3B_2$
		$^3\Sigma^-$	$^3B_1,^3B_2$
V^{2+} (d^3)	^4F	$^4\Phi$	$^4B_1,^4B_2$
		$^4\Delta$	$^4A_1,^4A_2$
		$^4\Pi$	$^4B_1,^4B_2$
		$^4\Sigma^-$	$^4B_1,^4B_2$
Cr^{2+} (d^4)	^5D	$^5\Delta$	$^5A_1(\sigma\pi^2\delta_-),^5A_2(\sigma\pi^2\delta_+)$
		$^5\Pi$	$^5B_1(\sigma\pi_y\delta^2),^5B_2(\sigma\pi_x\delta^2)$
		$^5\Sigma^+$	$^5A_1(\pi^2\delta^2)$
Mn^{2+} (d^5)	^6S	$^6\Sigma^+$	$^6A_1(\sigma\pi^2\delta^2)$

TABLE 3: Composition of the ^3F (d^2) Terms, Using Real Orbitals in C_{2v} and $C_{\infty v}$ Symmetry

state		
$C_{\infty v}$	C_{2v}	orbital structure
$^3\Sigma^-$ (^3F)	$^3A_2$	$\frac{1}{\sqrt{5}}\lvert\delta_+\delta_-\rangle - \sqrt{\frac{4}{5}}\lvert\pi_x\pi_y\rangle$
$^3\Pi_x$ (^3F)	$^3B_1$	$\sqrt{\frac{2}{5}}\lvert\sigma\pi_x\rangle - \sqrt{\frac{3}{5}}\left\lvert\frac{\pi_x\delta_+ + \pi_y\delta_-}{\sqrt{2}}\right\rangle$
$^3\Pi_y$ (^3F)	$^3B_2$	$-\sqrt{\frac{2}{5}}\lvert\sigma\pi_y\rangle + \sqrt{\frac{3}{5}}\left\lvert\frac{\pi_x\delta_- - \pi_y\delta_+}{\sqrt{2}}\right\rangle$
$^3\Delta_+$ (^3F)	$^3A_1$	$\lvert\sigma\delta_+\rangle$
$^3\Delta_-$ (^3F)	$^3A_2$	$\lvert\sigma\delta_-\rangle$
$^3\Phi_x$ (^3F)	$^3B_1$	$\frac{1}{\sqrt{2}}\lvert\pi_x\delta_+ - \pi_y\delta_-\rangle$
$^3\Phi_y$ (^3F)	$^3B_2$	$\frac{1}{\sqrt{2}}\lvert\pi_x\delta_- + \pi_y\delta_+\rangle$

TABLE 4: Composition of the ^4F (d^3) Terms, Using Real Orbitals in C_{2v} and $C_{\infty v}$ Symmetry

state		
$C_{\infty v}$	C_{2v}	orbital structure
$^4\Sigma^-$ (^4F)	$^4A_2$	$\lvert\sigma\left(\sqrt{\frac{4}{5}}\lvert\delta_+\delta_-\rangle + \sqrt{\frac{1}{5}}\pi_x\pi_y\right)\rangle$
$^4\Pi_x$ (^4F)	$^4B_1$	$\sqrt{\frac{2}{5}}\lvert\pi_y\delta_+\delta_-\rangle - \sqrt{\frac{3}{5}}\left\lvert\sigma\left(\frac{\delta_+\pi_x + \delta_-\pi_y}{\sqrt{2}}\right)\right\rangle$
$^4\Pi_y$ (^4F)	$^4B_2$	$-\sqrt{\frac{2}{5}}\lvert\pi_x\delta_+\delta_-\rangle + \sqrt{\frac{3}{5}}\left\lvert\sigma\left(\frac{\delta_+\pi_y - \delta_-\pi_x}{\sqrt{2}}\right)\right\rangle$
$^4\Delta_-$ (^4F)	$^4A_2$	$\lvert\pi_x\pi_y\delta_+\rangle$
$^4\Delta_+$ (^4F)	$^4A_1$	$\lvert\pi_x\pi_y\delta_-\rangle$
$^4\Phi_x$ (^4F)	$^4B_1$	$\frac{1}{\sqrt{2}}\lvert\sigma(\delta_+\pi_x - \delta_-\pi_y)\rangle$
$^4\Phi_y$ (^4F)	$^4B_2$	$\frac{1}{\sqrt{2}}\lvert\sigma(\delta_+\pi_y - \delta_-\pi_x)\rangle$

antibonding mix of the H_2 σ_g orbital. If the metal orbital is filled the stabilization because of the bonding interaction is offset by the concomitant antibonding interaction. Figure 2 shows the $6a_1$ bonding orbital in the $^2B_2$ state of ScH_2^{2+} in which the $3d_\sigma$ orbital is empty, and consequently, there is not a concomitant destabilization. Figure 3 shows the situation in the $^6A_1$ state of MnH_2^{2+} in which the $3d_\sigma$ orbital is occupied. One sees that the $3d_\sigma$ occupation forces a node that offsets the bonding stabilization. In Sc^{2+}, the four lowest states correlate to magnetic sublevels in which the $3d_\sigma$ orbital is empty, whereas the $^2A_1$ state in which this orbital is occupied has a significantly higher energy. In CrH_2^{2+} only, the $^5A_1(\pi^2\delta^2)$ does not have an occupied $3d_\sigma$, and it is significantly lower than the remaining states. Additional stabilization obtains when the metal has an occupied $3d\pi_y$ that can donate electrons into the σ_u antibonding orbital of H_2. This effect is illustrated in Figure 4 for the $3b_2$ orbital in the $^6A_1$ state of MnH_2^{2+}. These effects have been identified[13] for the corresponding MH_2^+ systems where they differ in degree, not kind. The remaining splitting patterns in Figure 1 may be understood in terms of these two effects.

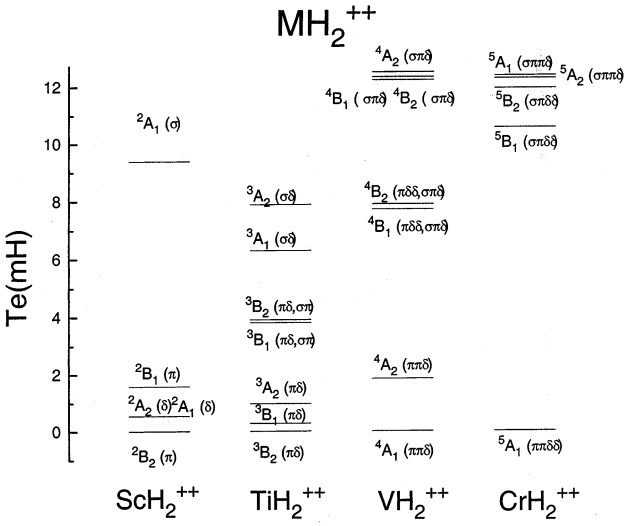

Figure 1. Energy levels of the low-lying electronic states of ScH_2^{2+}, TiH_2^{2+}, VH_2^{2+}, and CrH_2^{2+}.

TABLE 5: Binding Energies, Geometries, and Vibration Frequencies for the Low-Lying States of ScH_2^{2+} Arising from the ^2D Term of Sc^{2+}

	$^2B_2(\pi)$	$^2A_1(\delta)$	$^2A_2(\delta)$	$^2B_1(\pi)$	$^2A_1(\sigma)$
θ (degree)	19.24	18.55	18.55	18.69	17.23
ScH (au)	4.326	4.475	4.476	4.432	4.793
H−H (au)	1.446	1.443	1.442	1.440	1.436
Sc−H_2 (au)	4.265	4.417	4.417	4.373	4.739
T_e (mh)	0.0	0.54	0.55	1.58	9.38
D_e (mh)	24.6	24.0	24.0	23.0	15.2
D_0 (mh)	21.2	20.8	20.6	19.71	12.3
ν (b_2) (cm^{-1})	893	861	876	861	773
ν (a_1) (cm^{-1})	4063	4069	4114	4109	4129
ν (a_1) (cm^{-1})	912	879	894	879	789

The energy change in the charge-transfer reaction $M^{2+} + H_2 \rightarrow M^+ + H_2^+$ is given by $\Delta E = D_0(H_2) - D_0(H_2^+) - IP_2(M) + IP(H)$ and is a linear function of the second ionization energy of the transition metal. Numerically one has $\Delta E = 15.43$ eV − $IP_2(M)$, and because IP_2 for Cr and Mn is 16.49 and 15.64 eV, respectively, the reaction is exothermic for these elements. Note

TABLE 6: Binding Energies, Geometries, and Vibration Frequencies for the Low-Lying States of TiH_2^{2+} Arising from the $^3F(d^2)$ Term of Ti^{2+}

	$^3B_2$ ($\pi\delta$)	$^3B_1$ ($\pi\delta$)	$^3A_2$ (π^2,δ^2)	$^3B_1$ ($\pi\delta,\sigma\pi$)	$^3B_2$ ($\sigma\pi,\pi\delta$)[a]	$^3A_1$ ($\sigma\delta$)	$^3A_2$ ($\sigma\delta$)
θ (degree)	20.01	19.94	20.14	19.50		18.34	18.34
TiH (au)	4.182	4.192	4.151	4.280		4.535	4.533
H−H (au)	1.453	1.452	1.452	1.450		1.445	1.445
Ti−H_2 (au)	4.118	4.129	4.087	4.218		4.477	4.475
T_e (mh)	0.0	0.28	0.97	3.81	3.85	6.29	7.88
D_e (mh)	28.4	28.1	27.4	24.6	24.5	22.1	20.5
D_0 (mh)	24.9	24.7	24.0	21.2	21.2	18.9	17.2
ν (b_2) (cm^{-1})	952	944	951	930		849	846
ν (a_1) (cm^{-1})	3998	4006	3978	4036		4076	4138
ν (a_1) (cm^{-1})	970	962	970	948		866	863

[a] MRCI did not converge. Estimate from MCSCF results.

TABLE 7: Binding Energies, Geometries, and Vibration Frequencies for the Low-Lying States of VH_2^{2+} Arising from the $^4F(d^3)$ Term of V^{2+}

	$^4B_1$ ($\pi^2\delta$)	$^4A_2$ ($\pi^2\delta$)	$^4B_1$ ($\pi\delta^2,\sigma\pi\delta$)	$^4B_2$ ($\pi\delta^2,\sigma\pi\delta$)	$^4B_1$ ($\sigma\pi\delta$)	$^4B_2$ ($\sigma\pi\delta$)	$^4A_2$ ($\sigma\delta^2$)[a]
θ (degree)	21.29	21.29	20.22	20.17	19.42	19.55	
VH (au)	3.956	3.957	4.152	4.162	4.308	4.282	
H−H (au)	1.462	1.462	1.458	1.458	1.453	1.454	
V−H_2 (au)	3.888	3.889	4.087	4.098	4.247	4.220	
T_e (mh)	0.0	1.8	7.7	7.9	12.2	12.3	13.2
D_e (mh)	36.9	35.0	29.2	29.0	24.6	24.5	23.8
D_0 (mh)	33.5	31.6	25.8	25.6	21.8	21.1	20.4
ν (b_2) (cm^{-1})	981	981	962	957	867	943	
ν (a_1) (cm^{-1})	3918	3916	3961	3959	3901	3974	
ν (a_1) (cm^{-1})	999	999	979	974	883	960	

[a] MRCI did not converge. Estimate from MCSCF result.

TABLE 8: Binding Energies, Geometries, and Vibration Frequencies for the Low-Lying States of CrH_2^{2+} and MnH_2^{2+} Arising from the $^5D(d^4)$ Term of Cr^{2+} and from the $^6S(d^5)$ Term of Mn^{2+}

	CrH_2^{2+}					MnH_2^{2+}
	$^5A_1$ ($\pi^2\delta^2$)	$^5B_1$ ($\delta^2\pi\sigma$)	$^5B_2$ ($\delta^2\lambda\sigma$)	$^5A_2$ ($\pi^2\sigma\delta$)	$^5A_2$ ($\pi^2\sigma\delta$)[a]	$^6A_1$ ($\sigma\pi^2\delta^2$)
θ (degree)	22.27	20.58	20.30	20.65		21.42
CrH (au)	3.823	4.100	4.145	4.078		3.957
H−H (au)	1.476	1.465	1.461	1.462		1.471
Cr−H_2 (au)	3.751	4.034	4.080	4.012		3.888
T_e (mh)	0.0	10.6	11.9	12.3	13.7	0.0
D_e (mh)	44.0	33.4	32.0	31.7	30.3	35.7
D_0 (mh)	40.4	30.0	27.9	27.6	26.2	32.3
ν (b_2) (cm^{-1})	1048	986	1009	1019		1025
ν (a_1) (cm^{-1})	3850	3906	4169	4148		3859
ν (a_1) (cm^{-1})	1066	1003	1027	1038		1043

[a] MRCI did not converge. Estimate from MCSCF results.

that the second IP of all of the remaining elements in the first transition series is greater than 15.43, and the charge exchange reaction for these elements will be considerably exothermic. Because one expects the stability of the electrostatic complexes in the latter half of the first transition series to be comparable to the first half, the charge exchange reaction will be thermodynamically favored for these latter ions.

Bonding

The calculated binding energy for the lowest state of each of the metal dihydrides is collected in Table 9, and as one might expect, the binding energy increases with increasing atomic number until one reaches Mn where the occupied $3d_s$ orbital forces a slight decrease. Also listed is the electrostatic energy calculated from

$$\Delta E_{es} = -\alpha_\perp q^2/2R^4 - \Theta q/2R^3$$

where $q = +2$ and R is the distance from M^{2+} to the midpoint of H_2, and we use the free molecule values,[4] $\alpha_\perp = 4.85$ au and $\Theta = +0.468$ au. From the plot of these energies in Figure 5, we see that the molecules are not bound as strongly as the electrostatics would predict and the difference is remarkably constant. This difference represents the Pauli repulsion between the closed shell H_2 and M^{2+}, and its insensitivity to M^{2+} is presumably because it consists of two opposing contributions. As the number of electrons on the metal increases, one expects the Pauli repulsion to increase, but as the atomic number of the metal increases, its electron density contracts, and one expects the repulsion to decrease. The compromise is that the repulsion is, on average, about 12 mh. Figure 6 shows a density difference plot for the $^2B_2$ state of ScH_2^{2+}. This plot is representative of all of the dihydrides and shows vividly the polarization of the electrons on H_2 from M^{2+}.

Geometries and Vibration Frequencies

In each of the dihydrides, the H_2 frequency correlates reasonably well with the binding energy and H_2 separation. The larger the binding energy, the larger the H_2 separation and the

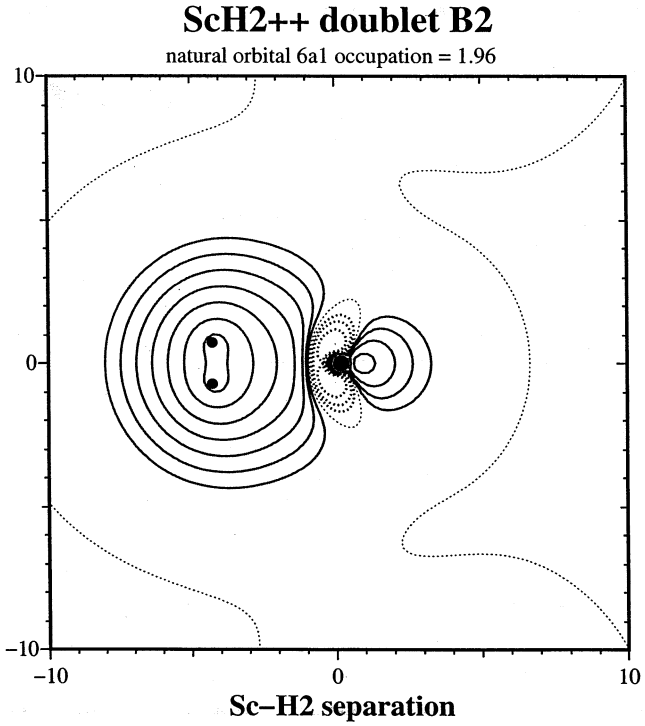

Figure 2. Amplitude of the $6a_1$ natural orbital in the $^2B_2$ state of ScH_2^{2+}. Contour levels are $\pm 2^N \times 10^{-2}$ au, with $N = -1, 0, 1, ..., 7$.

smaller, in general, the H_2 frequency. This obtains because of the donation from the H_2 s_g orbital to the metal $3d_s$ and the delocalization of the metal 3d orbital into the s_u orbital of H_2. The H_2 bond length and vibration frequency calculated at the MRCI level using the AVQZ basis are 1.402 a_0 and 4401 cm^{-1} in excellent agreement with the experimental values of 1.400 a_0 and 4400 cm^{-1}. We plot in Figure 7 the H_2 frequency shift versus the H_2 bond length increase in the ground state of each hydride. The correlation is quite remarkable especially that MnH_2^{2+} falls on the curve.

It's of interest to ask how much of the H_2 frequency shift is due to the mass differences between the metals. If the M−H force constant is k_r and the H−M−H force constant is k_θ the asymmetric stretch (b_2) frequency is given by

$$\sqrt{B(k_r/m_H)}$$

where m_H is the mass of a Hydrogen atom and

$$B = 1 + (2m_H/m_M)\sin^2(\theta/2)$$

where θ is the H−M−H angle. The two a_1 frequencies, ω_1 and ω_2, are given by the equations

$$\omega_1^2 + \omega_2^2 = (k_r/m_H)A + 2(k_\theta/m_H R^2)B$$

and

$$\omega_1^2\,\omega_2^2 = 2(k_r/m_H)(k_\theta/m_H R^2)C$$

where

$$A = 1 + (2m_H/m_M)\cos^2(\theta/2)$$

and

$$C = 1 + 2m_H/m_M$$

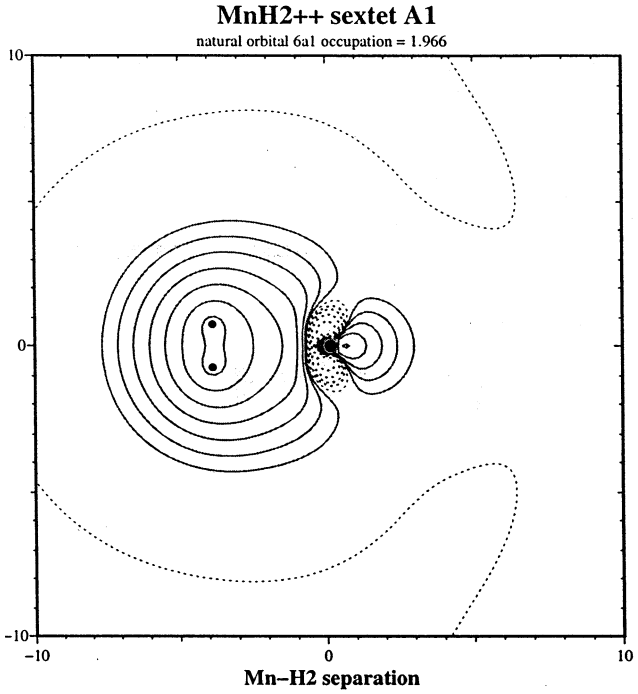

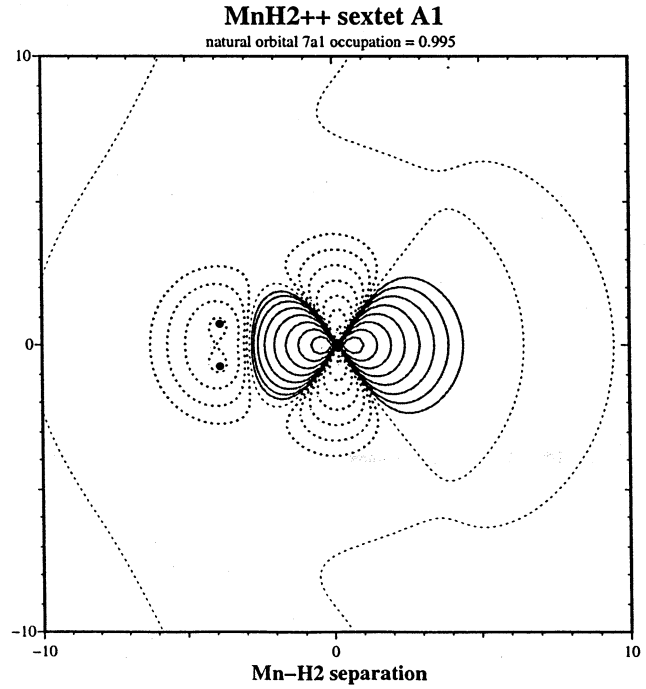

Figure 3. Amplitude of the $6a_1$ and $7a_1$ natural orbitals in the $^6A_1$ state of MnH_2^{2+}. Contour levels are as in Figure 2.

As m_M goes to ∞, $A = B = C = 1$ and the b_2 frequency and one of the a_1 become equal to

$$\sqrt{k_r/m_H}$$

whereas the a_1 corresponding to the H_2 vibration becomes

$$\omega_1 = \sqrt{2k_\theta/m_H R^2}$$

with k_θ/R^2 being the H_2 stretching force constant. Calculating ω_1 from this equation results in frequencies that differ by approximately 2 cm^{-1} from the coupled results, so the mass of

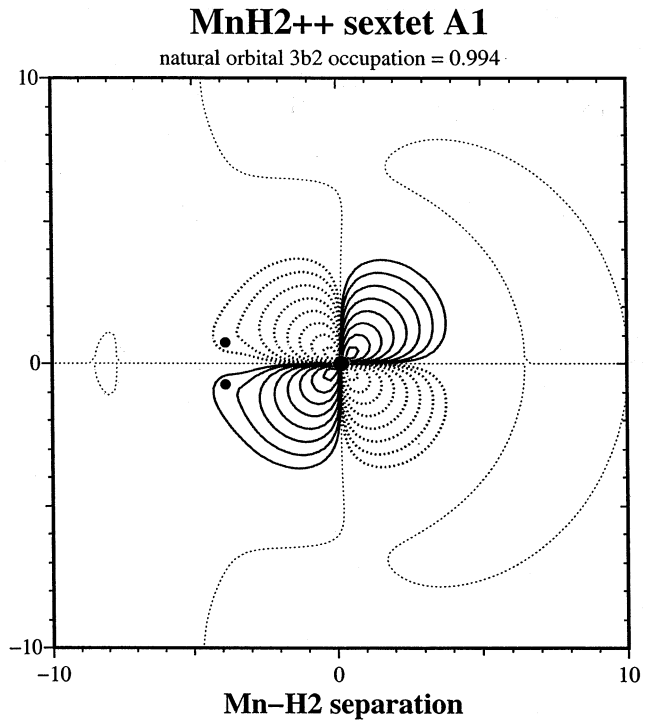

Figure 4. Amplitude of the $3b_2$ natural orbital in the $^6A_1$ state of MnH_2^{2+}. Contour levels are as in Figure 2.

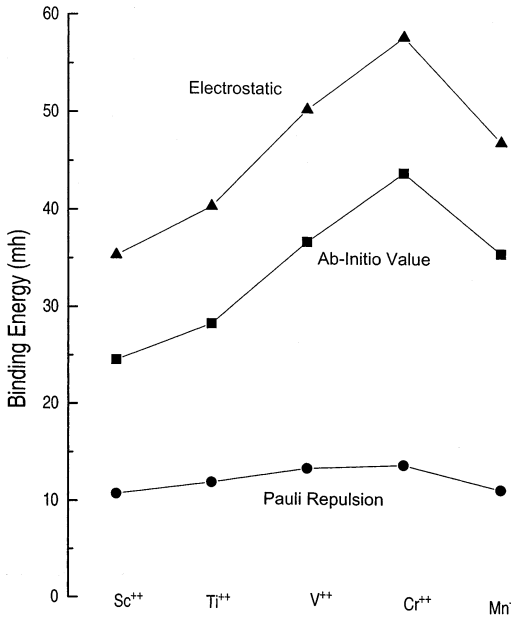

Figure 5. Binding energies in mh of the lowest state of MH_2^{2+}.

the metal has little effect on the H_2 frequency. Additionally, the approximate equality of the remaining two frequencies is seen to be a consequence of the relatively large mass of the metal.

Comparison with Monopositive Dihydrides

The mono and dipositive dihydrides differ in the in situ character of the metal. In the monopositive systems, one has a competition between the sd^n and d^{n+1} configurations of M^+, whereas the sd^n configuration in M^{2+} is several eV above the ground d^{n+1} configuration, and the 4s orbital plays little role in the bonding. This is reflected in the smoothly varying binding energies, H_2 vibration frequency, and geometry of MH_2^{2+} as

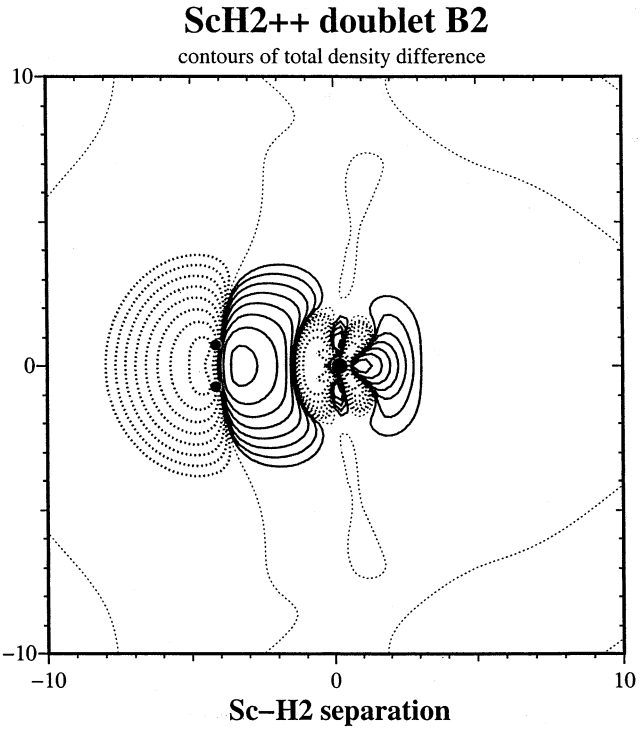

Figure 6. Amplitude of the density difference in the $^2B_2$ state of ScH_2^{2+}. Contour levels are $\pm 2^N \times 10^{-4}$ au, with $N = 0, 1, ..., 7$. Solid lines represent an increase in electron density relative to separated Sc^{2+} and H_2.

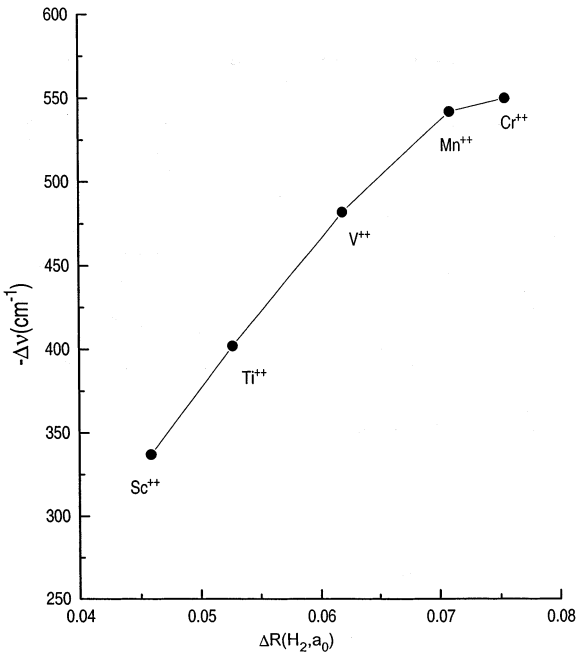

Figure 7. Plot of the decrease in the vibration frequency of H_2 (relative to free H_2) in the lowest state of MH_2^{2+} versus the increase in the H_2 separation (relative to free H_2).

shown in Tables 10 and 11. A detailed comparison is complicated because the geometries and frequencies of MH_2^+ are the results of DFT calculations with a somewhat smaller basis set than used in this work. However, it seems likely that the metal H_2 separation in Ti^+-H_2 is significantly smaller than in $Ti^{2+}-H_2$ because of the larger role played by the metal 4s electron in the Ti monopositive ion. The H_2 separation and frequency in these two ions is consistent with this interpretation. The 4s electron plays a somewhat smaller role in V^+- H_2 and this is

TABLE 9: Binding Energy (kcal/mol) in Lowest State of MH_2^{2+}

system	state	D_e	D_0	electrostatic	Pauli repulsion
ScH_2^{2+}	$^2B_2$	15.4	13.3	22.2	6.8
TiH_2^{2+}	$^3B_2$	17.8	15.6	25.4	7.6
VH_2^{2+}	$^4A_1$	23.1	21.0	31.6	8.5
CrH_2^{2+}	$^5A_1$	27.6	25.4	36.3	8.7
MnH_2^{2+}	$^6A_1$	22.4	20.3	29.6	7.2

TABLE 10: Comparison of MH_2^+ and MH_2^{2+} Binding Energies, D_0 (kcal/mol)

metal	MH_2^+ (exp)	MH_2^{2+} (theory)
Sc		13.3
Ti	10.0[a]	15.6
V	10.2	21.0
Cr	7.6	25.4
Mn	1.9	20.3

[a] Relative to $Ti^+(^4F(3d^3))$

TABLE 11: Comparison of Calculated Geometry and H_2 Frequency for MH_2^+ and MH_2^{2+}

	R (H_2) a_0		R (M−H_2) a_0		ν (H_2) cm^{-1}	
metal	MH_2^+	MH_2^{2+}	MH_2^+	MH_2^{2+}	MH_2^+	MH_2^{2+}
Sc		1.446		4.265		4063
Ti	1.474[a]	1.453	3.799[a]	4.118	3848[a]	3998
V	1.461[b]	1.462	3.683[b]	3.888	3936[b]	3918
Cr	1.474[c]	1.476	3.73[c]	3.751	4045[c]	3850
	1.437[d]		3.958[d]			
Mn	1.451[e]	1.471	4.575[e]	3.888	4258[e]	3859

[a] Reference 13. [b] Reference 11. [c] Reference 14. [d] Reference 5. [e] Reference 15.

reflected in the smaller difference in the mono and dipositive Vanadium complexes.

Acknowledgment. J.F.H. acknowledges the NSF equipment Grant, CHE-9974834, used to purchase the SGI Origin 3400 used in this work. J.P.K acknowledges the NSF REU program for support during summer 1999. Much of this work was done while J.P.K. was enrolled in Chemistry 499, *Chemical Physics Seminar*, at Michigan State University. J.F.H. thanks a referee for several very useful observations.

References and Notes

(1) Alvarado-Swaisgood, A. E.; Harrison, J. F.; *J. Phys. Chem.* **1985**, *89*, 5198.
(2) Rappe, A. K.; Upton, T. H. *J. Chem. Phys.* **1986**, *85*, 4400.
(3) Mavridis, A.; Harrison, J. F. *J. Chem. Soc., Faraday Trans.* **1989**, *85*, 1391.
(4) Rivera, M.; Harrison, J. F.; Alvarado-Swaisgood, A. E. *J. Phys. Chem.* **1990**, *94*, 6969.
(5) Bauschlicher, C. W.; Partridge, H.; Langhoff, S. R. *J. Phys. Chem.* **1992**, *96*, 2475.
(6) Maitre, P.; Bauschlicher, C. W. *J. Phys. Chem.* **1993**, *97*, 11912.
(7) Kemper, P. R.; Bushnell, J.; von Helden, G.; Bowers, M. T. *J. Phys. Chem.* **1993**, *97*, 52.
(8) Bushnell, J.; Kemper, P. R.; Bowers, M. T. *J. Phys. Chem.* **1993**, *97*, 11628.
(9) Bushnell, J.; Kemper, P. R.; Maitre, P.; Bowers, M. T. *J. Am. Chem. Soc.* **1994**, *116*, 9710.
(10) Bushnell, J.; Kemper, P. R.; Bowers, M. T. *J. Phys. Chem.* **1995**, *99*, 15602.
(11) Maitre, P.; Bauschlicher, C. W. *J. Phys. Chem.* **1995**, *99*, 6836.
(12) Bauschlicher, C. W.; Maitre, P. *J. Phys. Chem.* **1995**, *99*, 34444.
(13) Bushnell, J.; Maitre, P.; Kemper, P. R.; Bowers, M. T. *J. Chem. Phys.* **1997**, *106*, 10153.
(14) Kemper, P. R.; Weis, P.; Bowers, M. T. *Int. J. Mass Spectrom. Ion Proc.* **1997**, *160*, 17.
(15) Weis, P.; Kemper, P. R.; Bowers, M. T. *J. Phys. Chem. A* **1997**, *101*, 2809.
(16) Kemper, P. R.; Weis, P.; Bowers, M. T.; Maitre, P. *J. Am. Chem. Soc.* **1998**, *120*, 13494.
(17) Kemper, P. R.; Weis, P.; Bowers, M. T. *Chem. Phys. Lett.* **1998**, *293*, 503.
(18) Bushnell, J. E.; Kemper, P. R.; von Koppen, P.; Bowers, M. T. *J. Phys. Chem.* A. **2001**, *105*, 2216.
(19) Harrison, J. F. *Chem. Rev.* **2000**, *100*, 679.
(20) Bauschlicher, C. W., Jr. *Theor. Chim. Acta* **1995**, *92*, 183.
(21) Partridge, H. J. *J. Chem. Phys.* **1989**, *90*, 1043.
(22) Kendall, R. A.; Dunning, T. H.; Harrison, R. J. *J. Chem. Phys.* **1992**, *96*, 6796.
(23) MOLPRO is a package of ab initio programs written by Werner, H.-J. and Knowles, P. J., with contributions from Almlof, J.; Amos, R. D.; Dugan, M. J. O.; Elbert, S. T.; Hampel, C.; Meyer, C.; Peterson, K.; Pitzer, R.; Stone, A. J.; Taylor, P. R.; Lindh, R.; Mura, M. E.; and Thorsteinsson, T.; University of Birmingham: Birmingham, AL, 1996.
(24) Davies, D. W. *Theory of the Electric and Magnetic Properties of Molecules*; Wiley: New York, 1967.
(25) Lawson, D. B.; Harrison, J. F. *J. Phys. Chem.* **1997**, *101*, 4781.